| Title | Fabrication of ordered, large scale, horizontally aligned Si nanowire arrays based on an in-situ hard mask block copolymer approach |
|---|---|
| Author(s) | Ghoshal, Tandra; Senthamaraikannan, Ramsankar; Shaw, Matthew T.; Holmes, Justin D.; Morris, Michael A. |
| Publication date | 2013-11-26 |
| Original citation | Ghoshal, T., Senthamaraikannan, R., Shaw, M. T., Holmes, J. D. and Morris, M. A. (2014) 'Fabrication of Ordered, Large Scale, Horizontally-Aligned Si Nanowire Arrays Based on an In Situ Hard Mask Block Copolymer Approach', Advanced Materials, 26(8), pp. 1207-1216. doi: 10.1002/adma.201304096 |
| Type of publication | Article (peer-reviewed) |
| Link to publisher's version | https://onlinelibrary.wiley.com/doi/abs/10.1002/adma.201304096 <br> http://dx.doi.org/10.1002/adma.201304096 <br> Access to the full text of the published version may require a subscription. |
| Rights | © 2013 WILEY-VCH Verlag GmbH & Co. KGaA, Weinheim. This is the peer reviewed version of the following article: Ghoshal, T. , Senthamaraikannan, R. , Shaw, M. T., Holmes, J. D. and Morris, M. A. (2014), Fabrication of Ordered, Large Scale, Horizontally-Aligned Si Nanowire Arrays Based on an In Situ Hard Mask Block Copolymer Approach. Adv. Mater., 26: 1207-1216., which has been published in final form at https://doi.org/10.1002/adma.201304096. This article may be used for non-commercial purposes in accordance with Wiley Terms and Conditions for Self-Archiving. |
| Item downloaded from | http://hdl.handle.net/10468/6779 |

UCC

University College Cork, Ireland
Coláiste na hOllscoile Corcaigh

**Fabrication of Ordered, Large Scale, Horizontally Aligned, Si Nanowire Arrays Based on an *Insitu* Hard Mask Block Copolymer Approach**

*Tandra Ghoshal,\* Ramsankar Senthamaraikannan, Matthew T. Shaw, Justin D. Holmes, and Michael A. Morris\**

----------------------------------------------------------------------------------------------------------

[\*] Corresponding Author: Prof. Michael A. Morris

E-mail: m.morris@ucc.ie

Tel: + 353 21 490 2180

Fax:  +353 21 427 4097

[\*] Corresponding Author: Tandra Ghoshal

E-mail: g_tandra@yahoo.co.in

Tel: + 353 21 490 2911

Authors: Ramsankar Senthamaraikannan, Justin D. Holmes

[1]Materials Research Group, Department of Chemistry and Tyndall National Institute, University College Cork, Cork, Ireland

[2]Centre for Research on Adaptive Nanostructures and Nanodevices (CRANN), Trinity College Dublin, Dublin, Ireland

Author: Matthew T. Shaw

[3]Intel Ireland Ltd., Collinstown Industrial Estate, Co. Kildare, Ireland

Abstract: We report a simple technique to fabricate horizontal, uniform Si nanowire arrays with controlled orientation and density at spatially well defined locations on substrate based on *insitu* hard mask pattern formation approach by microphase separated polystyrene-b-poly(ethylene oxide) (PS-b-PEO) block copolymer (BCP) thin films. The methodology may be applicable to large scale production. Ordered microphase separated patterns of the BCP were defined by solvent annealing and the orientation was controlled by film thickness and annealing time. Films of PEO cylinders with parallel orientation (to the surface plane) were applied to create 'frames' for the generation of inorganic oxide nanowire arrays. These PEO cylinders were subject to selective metal ion inclusion and subsequent processing was used to create iron oxide nanowire arrays. The oxide nanowires were isolated, of uniform diameter and their structure a mimic of the original BCP nanopatterns. The phase purity, crystallinity and thermal stability of the nanowires coupled to the ease of large scale production may make them useful in technological applications. Here, we demonstrate that the oxide nanowire arrays could be used as a resist mask to fabricate densely packed, identical ordered, good fidelity silicon nanowire arrays on the substrate. The techniques may have significant application in the manufacture of transistor circuitry.

The computer processor industry is facing a number of challenges in defining 1D (nanowire) structures at substrate surfaces.[1] These challenges are related to lithographic and etch limitations and, in particular, the need to use double or triple patterning to create 1D features for use in logic or interconnect circuitry. Advances in extreme UV lithography have been slow and costs are spiralling. Directed self-assembly (DSA) where arrays of nanowires can be created by a combination of spontaneous arrangement of materials and 'directing' forces which force the patterns into alignment with a surface feature/direction.[1] The most promising technique appears to be the DSA of block copolymers (BCPs) which have been shown to form a number of highly regular nanostructure arrangements due to the thermodynamic incompatibility of the blocks by a process known as microphase separation where the interfacial energies of the solid substrate and the air interface contribute appreciably to the equilibrium free energy.[2-5] Many strategies have been investigated to manipulate interfacial interactions, to obtain a specific orientation and/or lateral ordering of the microdomains including external fields (magnetic, electrical), sample temperature gradient, mechanical effects such as rubbing and substrate topographical and chemical patterns.[6-9] Spin coating and solvent annealing is an efficient approach where ordering can be achieved in short time periods under solvent atmospheres since the solvent swells the polymer, creating free volume and providing the necessary chain mobility to the polymer blocks to facilitate self-assembly.[10-11] In particular, control over microdomain orientation is dictated by a complex interplay of surface energies, polymer-solvent interactions, and the commensurability between the film thickness.[12] The delivery of BCP lithography would not only afford means of extending logic device feature size reduction but might also promise cost-effective means of generating applications such as flexible electronic devices and sensors.

However, whilst BCP lithography has been demonstrated for the definition of horizontally (to the surface plane) orientated and aligned nanowire structures,[13-15] a number of challenges exist. Amongst these are: the ultimate feature size attainable, definition of the pre-patterns, defect density etc. Lamellar forming diblock BCPs (DBCPs) are favoured because of the ease of pattern transfer but are challenging because this phase is particularly sensitive to the interfacial energies of the substrate surface and the air interface.[16-18] Further, lamellar forming, small feature size DBCPs appear to be few in number. The cylindrical phase appears to be more easily controlled since interfacial energy control is less demanding, however, the pattern transfer of this structure is extremely challenging because of the distribution of one block in a matrix of the other and the small diameter of the cylinders.[19-21] For vertically orientated cylindrical phase systems, we have demonstrated that thin films of DBCP can be used to create vertical nanowire structures by a method of oxide inclusion to allow formation of a hard mask.[22-23] These structures are amenable to material modification because both blocks are present at the surface. Less clear is how horizontally aligned cylinders may be modified by techniques such as nanoparticle decoration or CVD.

Here we report the first application of an inclusion technique that allows selective infill of a cylindrical structure such that continuous wires can be formed across a substrate surface. We have further showed that this can be used to generate oxide hard mask arrays to transfer to the substrate and form silicon nanowires. A number of difficulties have been met and dealt with including: creation of single cylinder structures over large area, fine tuning of the inclusion methodology to yield high quality nanowire structures and proper characterization of the ultra-small features formed. The work clearly demonstrates that cylindrical structures may be used to form high quality horizontal 1D silicon nanopatterns for logic/interconnect applications. We also assert that it will enable the application of nanowire based technologies in many other areas.

The block copolymer employed in this study is Polystyrene-b-poly(ethylene oxide) (PS-b-PEO) (42k-11.5k) with PEO as the minority cylinder forming block. To control the structure of the film and properly define parallel orientated cylindrical structures, careful control of the annealing solvent and film thickness were required. The ellipsometry measured film thicknesses were 40 nm, 72 nm and 108 nm for 1, 2 and 3 wt% polymer solution concentrations respectively. **Figure 1** summarizes the microdomain structure formation as functions of solvent anneal times for each different film thicknesses. A hexagonally ordered structure is indicated in all of the AFM images. After 30 minutes solvent annealing, the PEO cylinders oriented normal to the substrate irrespective of film thicknesses (Figures 1a, d, g). The repeat period calculated from the fast-Fourier transform (FFT) of the AFM images is 42 nm and this value (+/- 2%) was observed for all films irrespective of orientation. When the anneal period is increased to 1 h, a hybrid morphology consisting of cylinders oriented both parallel and perpendicular to the surface plane is observed but note that the fraction of parallel cylinders increases with increasing film thickness as shown in the inset of Figures 1a, d, g. For the thickest film (3%), nanosized triangular islands of different thickness can be seen (inset of Figure 1g). For the thin film (1%), parallel orientation is predominant after 1h 30 min (not shown) but perpendicular domains were still present. Complete parallel orientation of the thinnest film was only observed at solvent exposure times of 2 h (Figure 1b) and 2h 30m (Figure 1c) and this is stable to 4h. For thicker films, parallel and perpendicular cylinders coexist with parallel orientation as a major assembly for longer annealing times (Figures 1e, f, h i). Compared to the thin films, large scale surface roughness or thickness undulation is noticed with longer solvent exposure (2h 30m) as shown in Figures 1f (5 x 5 μm) and 1i (4 x 4 μm). The thickness dissimilarity and wavy nature of the surface is evident from the combination and differences in the colours of the film surfaces by the microscopic images for the films annealed for 2h 30m (see supporting information). Hence

thinner films exhibit lower defect densities and smoother surface compared to the thicker films at similar temperature.

It should be noted that the PS-b-PEO system is complex as the blocks exhibit asymmetric affinities for the solid substrate and the air interface. Previous works suggests that the hydrophilic PEO will preferentially wet the substrate surface (favourable PEO-substrate interactions) whilst PS will segregate to the air interface to form a PS-rich layer (PS has a lower surface energy, $\gamma_{PS}$ = 33 mNm$^{-1}$; $\gamma_{PEO}$ = 43 mNm$^{-1}$).[24] Although PEO dissolves in toluene, the toluene is a selective solvent for PS since the solubility parameter difference with PS is much smaller ($\delta_{Tol} - \delta_{PS}$ = 18.3-18 =0.3 MPa$^{1/2}$) than PEO does ($\delta_{Tol} - \delta_{PEO}$ = 18.3-20.2 =1.9 MPa$^{1/2}$). In order to ensure complete diffusivity of toluene through the PS matrix, [11] the solvent anneal temperature used was optimized at 60$^{0}$ C, which is just above the melting temperature of the PEO block (55$^{0}$ C) for this particular molecular weight system. Thus, PEO is in a semi-molten state during annealing and this probably explains some the ease with which the system re-orientates and changes morphology during annealing, simultaneously lower diffusivity and high viscosity of the domains facilitate the same translational order.

This information may be used to explain the observations here. Short-period solvent annealing gives a vertical orientation because this represents the least entropically hindered route to microphase separation, since the PEO cylinder length is limited to the thickness of the films. However, at extended periods this phase can relatively easily re-orientate into a parallel orientation which although entropically less favoured allows PS to form the majority surface block and minimize the free energy of the system. The parallel orientation is favoured at the correct monolayer (relative to cylinder repeat distance). Clearly, the thinnest film shows the greatest tendency to produce a stable parallel arrangement whilst thicker films show increased likelihood of forming mixed orientations. For relatively thicker films, the internal morphology is unknown and the surface patterns may not essentially be propagated

through the entire film thickness. Because the substrate oriented interfacial layer should be separated from the region far above where ordering should be dominated by the polymer-air interface where the mixed morphologies may coexist in the interfacial layer. **Scheme 1** demonstrates the equilibrium surface patterns, thicknesses and internal morphology for different concentrations of polymers for longer annealing time (2h). A simple explanation of this observation is that thermodynamics become less favourable to the parallel orientation as thickness increases.[25] Instead, the increased roughness (a direct result of having non-ideal thickness) will favour parallel arrangements in regions where film thickness is ideal and vertical orientation in non-ideal circumstances.

It is noted that the larger free energy for a monolayer film compared to a multilayer film[25] can cause frequent structural transition in order to release the extra tension. Residual solvent may also be of importance here to explain stable surface pattern morphology for thinner films for longer annealing times. The trapping of solvent (toluene) in the solvent annealed films due to the vitrification of the film during solvent removal can have significant effects.[26] The trapped solvent may cause defects in the surface morphology and also modify the polymer-substrate, polymer-air and polymer-polymer interactions. The increased order and the uniformity of pattern orientation for the thinnest films could be due to significantly less residual solvent and lack of a well-defined solvent front. For thicker films, longer time is required to evaporate the solvent due to combined effects of sufficiently large film thickness and attractive interaction of the solvent with the substrate.[27] The presence of significant solvent in thicker films may also help to form the island type structure observed (e.g. in the inset of Figure 1g small triangular islands of area $\sim$ 40-80 nm$^2$ and average height about 2-3 nm are readily formed) due to solvent enhancing the large mass transport required. On extended solvent annealing, larger islands form presumably following two dimensional Ostwald ripening type mechanisms (Figure 1h).

As previously shown for vertically orientated hexagonally arranged cylinder structures of this BCP system in order to include inorganic materials it is necessary to activate the PEO, a process that leads to removal and densification of the PEO domains to produce nanopores.[22, 24] Chemical degradation and/or modification of the PEO blocks were achieved through ultrasonication or simply immersing the film at a certain temperature in anhydrous ethanol. Both the processes are efficient but the immersion process is time-consuming. Since ethanol is a non-selective solvent for PS, this suggests that in the horizontally aligned films developed here that at least parts of the PEO cylinders are exposed at the film surface. **Figure 2** shows the AFM and SEM images of the PS-b-PEO systems of different thicknesses BCP films after ultrasonic ethanol treatment (similar for all films). The long-range order, periodicity and spacing (cylinder spacing = 42 nm and PEO cylinder diameter = 18 nm) of the BCP pattern are essentially unchanged by this process. Topographic AFM images (Figures 2a-c) demonstrate contrast enhancement following ethanol ultrasonic treatment. No thickness change on ethanol treatment was observed for the respective films as measured by ellipsometry. No deformation or discontinuity of the nanoporous template was observed. The process is effective for a variety of PEO cylinder lengths formed under different solvent annealing time (see supporting information). Inset of Figure 2a demonstrate nanoporous line-like pattern over an extended area (2 x 2 μm). Figure 2d demonstrates that the treatment is equally effective for films of mixed cylinder orientation.

It should be noted that the ethanol exposure time had to be carefully optimized as longer exposures/higher temperatures resulted in surface roughness or structural degradation of the film. Figure 2e depicts the morphology of the polymer film (1%) after the ethanol immersion for 14 h. The cylinders are become discontinuous and swollen suggesting initial film decomposition and intermediate stage of the modification. In the case of the thicker films (3%, 24 h ethanol treatment, Figure 2f), the film consists of different layers of cylinder

arrangements where films in different layers are no longer parallel. It is apparent that the longer exposure removed regions of the upper cylinder layers whilst allowing movement of the layers. The same discontinuities as seen in Figure 2e are also observed.

The ability to produce high contrast SEM images for the 1% and 2% polymeric films (Figures 2g and h respectively) also suggest a height variation across the surface and modification/removal of the PEO. This is confirmed by cross-sectional SEM images in Figure 2i for 1% polymeric film after ethanol treatment. The images were taken from different area of the film and the contrast was adjusted to reveal the underneath polymer layer on top of Si substrate (top image) and the 'missing' PEO cylinders (bottom image). The measured thickness of the template is 40 nm, in close agreement with ellipsometry measurements. We suggest a PS contact layer exists at the substrate interface below the missing cylinders which is further confirmed by TEM (below).

Either the ultrasonic treatment or a certain temperature is required to create the nanoporous templates for the generation of oxide nanostructures. The ethanol treatment process requires comment as acid treatments are normally used for reconstruction or etching of these systems.[21, 28] Here, ethanol was preferred as an etching solvent because of its' vapour pressure, selected solubility into PEO (since they have similar solubility parameters) and chemistry. We suggest that the acoustic cavitation during ultrasonication generates free radicals for bond cleavage of the PS-PEO bond. Acoustic cavitation is more aggressive in solvents with a lower vapour pressure (5.95 kPa at $20^0$ C).[29] It was also found that ethanol was the most appropriate of the alcohols. This might suggest that the similarity of the chemical structures of PEO monomers [$(CH_2CH_2O)$-] and ethanol molecules ($H$-$CH_2CH_2O$-$H$) is important. In this way, the ethanol is highly effective in dissolving PEO fragments and also providing an ideal solvent to allow crystallization of the PEO.[24] When ultrasound was ceased, the PEO molecules would prefer to separate from the solution but cannot because

those PEO monomers and ethanol molecules cannot distinguish from each other, as a result, the PEO chains are frustrated and have no choice to form a thin crystalline layer when there is still some ethanol molecules present in the adjacent regions. Thus, the layer section consists of both ethanol and crystalline PEO as some ethanol is confined within the crystalline PEO layer.[30] This is why it is important to take out the film from the solution and dry it as quickly as possible.

Careful Cross-sectional TEM helps to resolve the morphology of these films (**Figures 3**a and b). Prior to ethanol treatment, (see supporting information) the similarity of the PS (1.05 g cm$^{-3}$) and amorphous PEO (1.12 g cm$^{-3}$) densities results in featureless TEM micrographs. This suggests that solvent annealing does not result in PEO crystallization even at a temperature higher than its melting point since the crystalline form has higher density (1.24 g cm$^{-3}$)[31] and might be expected to provide TEM contrast.[32] For both the thickest (3%, Figure 3a) and thinnest (1%, Figure 3b) films indicate that the cylinders affected by the ethanol treatment are located at the exterior surface. It is also clear that the interior PEO domains below the surface are not altered by the ethanol treatment. The polymer film shows no indication of deformation or delamination at the substrate interface and the TEM derived thicknesses of 113 nm and 40 nm (3% and 1% respectively) are consist with ellipsometry measurements. In the 3% film, a few elliptical areas within the film can be seen and these are at a similar repeat distance (42 nm) as the cylinder spacing observed above (Figure 3a). We asset these are crystalline PEO cylinders that are deformed by in plane surface strain[33] that demonstrate multilayer formation. Note these are only visible if they are in the correct orientation in the TEM lamellae. We believe some crystallization can occur at 40$^0$C[31] and the elliptical regions appear due to the density or contrast enhancement. The 'nanopores' formed by ethanol treatment are a consistent depth of 17 nm across the film. Higher magnification images (insets of Figures 3a and b) give an average PEO width of 18 nm

consistent with top-down images and suggesting that cylinders at the surface are not subject to significant strain. It was not possible to detect the thin layer section within the nanopores because of thicker platinum layer. Compared to the thin film, a very thick layer (96 nm) exists underneath the porous structures consisting of both PS and PEO. Whereas only a 23 nm non-porous PS layer exists on top of the Si substrate as has been suggested before.[22]

XPS analyses were performed to provide further understanding of the ethanol process for the 1% film. The C1s peaks can be curve-fitted to reveal four components as illustrated in Figures 3c and 3d. Two of these can be attributed to carbon from the aromatic ring of PS (**C**-(C,H)$_{arom}$) and the aliphatic backbone of PS (**C**-(C,H)$_{aliph}$) at 284.9 eV and 285.3 eV respectively. A distinct high binding energy shoulder on the primary C1s peak can be seen particularly for the untreated sample and this is assigned to carbon involved in an ether link (**C**-O-**C**) from PEO at about 286.6 eV. A shake-up satellite assigned to the aromatic ring of PS (**C**$_{sh\ up}$) at about 291.8 eV was also seen. From the total C1s peak area (includes adventitious signal), the calculated contribution of PEO component decreases from 28% to 9% after the ethanol treatment. This is consistent with PEO degradation but also suggests that some PEO remains possibly in a crystalline form.

The nanoporous line templates can be used to create ordered oxide nanowire arrays by the metal inclusion method through spin coating the precursor-ethanolic solution and subsequent UV/Ozone treatment. Following our previous work,[23] where it was reported that iron oxide nanodots can be an excellent resistant mask for high aspect ratio silicon substrate patterning. Attempts were made to adopt this strategy to produce silicon nanowire arrays by use of the oxide wires as a hard mask. As shown below, the thinnest BCP film thicknesses produce the best nanowire arrays.

**Figures 4**a-c represents the AFM images of the iron oxide nanowires prepared using the templates of thicknesses 40 nm, 72 nm and 113 nm respectively using an equivalent amount

of precursor solution. For the 40 nm films, ordered large area nanowire arrays were realized with uniform size/shape and their arrangement mimics that of the original BCP patterns (Figure 4a). The average diameter of the nanowires is 16 nm and equal throughout the entire length. For the thicker films, a few nanowires are seen in discrete areas but irregular, disconnected and agglomerated nanowire assemblies are dominant (Figures 4b, c and f). Further, nanowires of varying diameter along their length are also seen. SEM images also confirm AFM observations as seen in Figure 4d. The thinner film clearly has well defined, large area nanowire arrays and the higher magnification image (inset of Figure 4d) reveals the continuous nature and smooth profile of the nanowires.

The nanowires formed using these methods are well-adhered to the substrate and thermally robust. Typical data (Figure 4e) show large area views of the arrays after air calcination at $800^0$C for 1 h. Higher magnification images reveals well isolated, monodispersed arrays with a centre to centre spacing of 42 nm (as previous). As might be expected, for thicker films, disconnected (2%) and entangled (3%) nanowires were formed after air calcination as shown in the insets of Figures 4f and c respectively.

It should be noted that the concentration of the iron precursor solution is critical and was carefully optimized (4.6 wt%) to obtain isolated and continuous nanowires (see supporting information). Figure 4g and inset shows the nanostructures formed with two different concentrations; lower concentration (4%) gave non-continuous nanowire-like structures whilst a 5% solution yielded an interconnected nanowire network.

The structural quality, composition and the interfaces were further analysed using FIB-thinned TEM cross-sections. The adhesion of the materials is reflected in the mechanical integrity (i.e. no interfacial cracks etc. at the interface of the wires with the substrate) of the structures during FIB processing. We suggest this approach offers advantages over lithographic patterning of a oxide film where interfacial tensions can result in delamination

and mechanical damage under strain.[34] The cross-sectional TEM image shows well-separated nanowires supported on the passive silica substrate surface (Figure 4h). The wires are crystalline (see supporting information) and of average diameter/height 15/6 nm respectively (as previously seen by AFM and SEM). Elemental composition was confirmed by high resolution EDAX mapping and the distribution of Fe, O and Si are shown in Figures 4i. The Fe map shows a homogeneous distribution of Fe corresponding to each nanowire and a sharp elemental interface to the substrate surface suggesting no inter-diffusion occurs. The O and Si maps confirm the presence of oxides on the nanowire and passive layer and the substrate.

The chemical composition of the iron oxide nanowires before (UV/Ozone alone) and after annealing was confirmed by Fe 2p XPS studies. Prior to annealing, the Fe 2p core level spectrum of the as-formed iron oxide nanowires (**Figure 5**a) consists of peaks at 711.1 eV (Fe $2p_{3/2}$ ) and 724.5 eV (Fe $2p_{1/2}$ ) which are broadened due to the presence of $Fe^{+2}$ and $Fe^{+3}$ ions. Curve-fitting using Gaussian-Lorentzian line shapes provides individual binding energies of 709.6/722.9 eV (assigned to $Fe^{+2}$) and 711.5/724.9 eV ($Fe^{+3}$) in agreement with literature assignments.[35] The $Fe^{+3}$/ $Fe^{+2}$ ratio was estimated to about 2:1 as expected for $Fe_3O_4$. Following calcination the Fe 2p core level spectrum (Figure 5b) consists of two sharp peaks at 711.4/725.2 eV corresponding to the Fe $2p_{3/2}$ and Fe $2p_{1/2}$ signals. A high binding energy satellite (+8 eV shift) can also be seen and these data are consistent with formation of $Fe_2O_3$.[36-37] A typical XPS survey spectrum (inset of figure 5b) of iron oxide nanowires after annealing confirms the expected presence of Si, O, C and Fe. The C1s feature is relatively small and demonstrates effective removal of carbon species during processing. Its intensity is consistent with adventitious material formed by adsorption and other contamination during sample preparation.

The metal ion inclusion into the nanoporous template is favoured by a combination of capillary forces and the affinity of PEO with the ionic ethanol solution. The spin coating procedure is highly efficient and it is suggested that the PEO-ethanol layer accelerates the metal ion inclusion process probably via either intra- or intermolecular coordination via electron donation from the PEO block to oxygen species in the ethanol molecule.[24] The effectiveness of this simple solution mediated inclusion is consistent with the spectroscopic data suggesting the presence of PEO after the ethanol treatment. Had complete removal of the PEO been achieved, it would be highly unlikely that significant metal uptake would occur because the PS matrix would be hydrophobic. For the thicker films, the underlying layer of the nanoporous template consists of both PS and PEO as suggested before and during spin coating, metal ions were incorporated only into the surface pores because the non-porous PEO cylinders underneath were protected by the PS matrix. In this case, UV/Ozone treatment cross-links the polymers, oxidizes the metal-complex, remove the polymer simultaneously and all these processes are kinetically controlled. The iron oxide nanostructures were interrupted while settles down to the substrate through the thick polymer layer. Increment of polymer layer thickness to a certain extent, the nanostructures experiences diameter variation, edge roughness and periodic irregularity.

In order to create Si nanowire structures on the substrate surface, the iron oxide nanowires were used as a hardmask in the ICP etch process. A mild oxalic acid aqueous solution was used to remove undesired $Fe_2O_3$ from the as-formed Si nanowire arrays. **Figure 6**a shows cross-sectional SEM image of Si nanowires over large substrate areas following a 1 min Si etch. A higher magnification image (inset of Figure 6a) demonstrate that the nanowires are continuous and of regular diameter (15 nm) along the length. The centre to centre nanowire spacing remained unchanged. This implies that the etching does not damage the original 'mask' to a significant extent. The depth of the nanowires can be varied by increasing the Si

etch time and Figures 6a-c represents the SEM images of the nanowire arrays following etches of 1-3 min. All the images reveal large scale fabrication of ordered continuous Si nanowires. As the etch time is increased pattern contrast is enhanced and the cross-sectional SEM data give approximate nanowire heights of 50, 100 and 150 nm for 1, 2 and 3 min etches respectively. In all cases, the cross-sectional SEM images show wires of uniform width (with height) and smooth sidewalls demonstrating the mask effectiveness. Note that further increases in etch time may results in nanowire discontinuity in few areas (see supporting information). It is not clear of this is due to etch degradation or mechanical weakness of the samples. To demonstrate the use of these for making silicon devices, the process was also demonstrated on silicon-on-insulator (SOI) substrates of 30 and 70 nm Si device layers using adjusted Si etch times of 30 and 70 s respectively. The top-down SEM reveals similar nanowire assembly on SOI (not shown). The iron oxide nanostructures prepared for lower and higher concentrations of precursors also shows significant contrast enhancement with identical pattern after the Si etch as shown in Figure 6d and inset. Thus, the fabricated Si nanopatterns were solely following the original mask patterns on Si substrate.

Cross-sectional TEM was used to fully characterize the nanowires. Figures 6e and f show micrographs of the array of 2 min etched nanowires on Si substrates following iron oxide removal. The images reveal nanowires of about 100 nm long as the expected 42 nm spacing. Contrast at the surface of the wires is seen due to the presence of the original passive layer or due to fluoride formation during etching.[23] All of the wires investigated had a rectangular profile with smooth sidewalls and there little variation of wire width along its' length as seen in the inset of Figure 6e. Note that the nanowires are unaltered by iron oxide removal. Importantly, the HRTEM image (Figure 6f) reveals a highly crystalline structure with no sign of etch related amorphortization. Note also that the lattice fringes are continuous between

bulk and nanowire silicon indicating no stacking or other defects and hence no re-crystallization during etching. The image in the inset of Figure 6f shows the lattice fringes with spacing 3.11 Å across the wires agrees reasonably well with Si fcc (111) interplanar distances.[38] The $54^0$ angle of the (111) fringes with the substrate surface plane is consistent with the (100) orientation of the Si wafer. Thus, highly dense uniform 1D silicon nanowire arrays with controlled crystallographic orientation could be created through selective etching of the silicon wafers of chosen orientations.

A schematic detailing the fabrication of the Si nanowires is shown in **Scheme 2**. Solvent annealing of the spin coated film (Scheme 2A) in toluene produces hexagonally arranged PEO cylinders parallel to the substrate in PS matrix (Scheme 2B). Modification of PEO cylinders creates nanoporous template for the metal ion inclusion (Scheme 2C). Iron oxide nanowires were prepared by spin coating metal ion precursor solution (Scheme 2D) followed by UV/ozone treatment to oxidize the precursor and remove the polymer (Scheme 2E). Si nanowires were fabricated by consecutive silica and silicon ICP etch processes (Scheme 2F).

In conclusion, We represents a simple and cost effective large scale fabrication of horizontal, uniform Si nanowire arrays with precise placement on substrate based on insitu hard mask microphase separated BCP approach. Hexagonally arranged self-assembled PS-b-PEO nanopatterns were realized by a simple solvent annealing process and the morphological evolution was investigated as function of film thickness and annealing time. This morphological variability is attributed primarily to the trapping of residual solvent (toluene) within the film and the differences in the interfacial energies between the polymer, air and the substrate. Compared to the thicker films, thin film of monolayer cylinders depicts uniform thicknesses and stable surface patterns throughout the film. An effective ethanol ultrasonication/immersion protocol for the degradation or modification of the PEO cylinders was developed to create templates for the generation of inorganic materials without pattern

damage. The films of PEO cylinders with parallel orientation were applied for the generation of iron oxide nanowire arrays based on a methodology of selective metal ion inclusion and subsequent Uv/Ozone treatment. Monolayer thin films are proven to generate large scale, uniform diameter and smooth sidewall, horizontal iron oxide nanowire arrays while disconnected oxide patterns formed with increasing the film thickness. The nanowires are structurally arranged in a mimic of the original self-assembled BCP pattern and show strong adherence to the substrate to high temperature. Large area, identical ordered, crystalline, horizontal Si nanowire arrays is fabricated with a smooth sidewall profile by using these iron oxide nanowires as a hard mask over silicon. This self-assembled hardmask nanolithography can be employed to fabricate as-made devices of electrically separated Si nanowires with controlled crystallographic orientation on SOI substrate which can be an important component in the manufacturing of nanoscale devices with high throughput and low cost.

**Experimental Section**

*Preparation of iron oxide nanowire arrays by block copolymers:* Polystyrene-b-poly(ethylene oxide) (PS-b-PEO) diblock copolymer was purchased from Polymer Source and used without further purification (number-average molecular weight, $M_n$, PS = 42 kg mol$^{-1}$, $M_n$, PEO = 11.5 kg mol$^{-1}$, $M_w/M_n$ = 1.07, $M_w$: weight-average molecular weight). Single crystal B doped P type silicon (100) wafers with a 10 nm silica layer were used as a substrate. Substrates were cleaned by ultrasonication in acetone and toluene for 30 minutes in each solvent and dried under nitrogen stream. PS-b-PEO was dissolved in toluene to yield 1, 2 and 3 wt% polymer solution and aged for 12 h at room temperature. The PS-b-PEO thin film was formed by spin coating the polymer solution (3000 rpm for 30 s). The films were exposed to toluene vapour placed at the bottom of a closed vessel kept at 60$^0$C for different time period to induce necessary chain mobility and allow microphase separation to occur. Partial etching and domain modification of PEO was carried out by ultrasonication of the

films for 20 min or immersing the film at $40^0C$ for 21 h in anhydrous alcohol. The ultrasonication treatment was carried out in Cole-Parmer ultrasonic cleaner 8891 which transform low-frequency AC current into 42 kHz high-frequency sound waves via a piezoelectric transducer. During ultrasonication, the solvent annealed films were placed at the bottom of a glass bottle filled with anhydrous alcohol at room temperature. After the desired time, the films were taken out from alcohol and dried immediately. For the fabrication of iron oxide nanowires, Iron (III) nitrate nonahydrate ($Fe(NO_3)_3,9H_2O$) was dissolved in ethanol and spin-coated onto the activated film. UV/Ozone treatment was used to oxidize the precursor and remove polymer. The thermal stability of the nanodots was verified by annealing them at $800^0C$ for 1 h.

*Pattern transfer using ICP etch:* These iron oxide nanowire arrays were used as a hard mask for pattern transfer to the substrate using an STS, Advanced Oxide Etch (AOE) ICP etcher as previously reported with the nanodot arrays.[23] The system has two different RF generators, one, to generate and control the plasma density by direct connection to the antenna coil, while the other one was used to adjust and control the energy of the ions by connecting it to the substrate holder. A double etching process was used to, firstly, etch the native silica layer and, secondly, the silicon substrate. During etching, the sample is thermally bonded to a cooled chuck ($10^0C$) with a pressure 9.5 Torr. For the oxide layer etch, the process parameters were optimised to a $C_4F_8/H_2$ gas mixture (21 sccm/30 sccm) using an ICP coil power of 800 W and a Reactive Ion Etching (RIE) power of 80 W. The silica etch time was kept constant (5 sec) for all the samples. For Si pillar fabrication, the process used a controlled gas mixture of $C_4F_8/SF_6$ at flow rates of 90 sccm/30 sccm respectively and the ICP and RIE power were set to 600 W and 15 W respectively at a chamber pressure of 15 mTorr.

*Characterizations:* Surface morphologies were imaged by scanning probe microscopy (SPM, Park systems, XE-100) in tapping mode and scanning electron microscopy (SEM, FEI

Company, FEG Quanta 6700 and Zeiss Ultra Plus). The film thicknesses were measured by optical ellipsometer (Woolam M2000) and electron microscopy. Samples were prepared for TEM cross sectional imaging with an FEI Helios Nanolab 600i system containing a high resolution Elstar™ Schottky field-emission SEM and a Sidewinder FIB column and were further imaged by transmission electron microscopy (TEM, JEOL 2100 and TEM, FEI Titan). X-Ray photoelectron spectroscopy (XPS) experiments were conducted on a Thermo K-alpha machine with Al $K_\alpha$ X-ray source operating at 72 W.

[1] Emerging research devices, *The International Technology Roadmap for Semiconductors*, 2011, 1.

[2] D. Borah, M. Ozmen, S. Rasappa, M. T. Shaw, J. D. Holmes, M. A. Morris, *Langmuir*, **2013**, *29*, 2809.

[3] Q. Wang, P. F. Nealey, J. J. de Pablo, *Macromolecules*, **2001**, *34*, 3458.

[4] S. Rasappa, D. Borah, C. C. Faulkner, T. Lutz, M. T. Shaw, J. D. Holmes, M. A. Morris, *Nanotechnology*, **2013**, *24*.

[5] D. Borah, M. T. Shaw, S. Rasappa, R. A. Farrell, C. O'Mahony, C. M. Faulkner, M. Bosea, P. Gleeson, J. D. Holmes, M. A. Morris, *J. Phys. D-Appl. Phys.*, **2011**, *44*, 174012.

[6] R. A. Segalman, H. Yokoyama, E. J. Kramer, *Adv. Mater.*, **2001**, *13*, 1152.

[7] T. Thurn-Albrecht, J. Schotter, C. A. Kastle, N. Emley, T. Shibauchi, L. Krusin-Elbaum, K. Guarini, C. T. Black, M. T. Tuominen, T. P. Russell, *Science*, **2000**, *290*, 2126.

[8] J. Y. Cheng, A. M. Mayes, C. A. Ross, *Nat. Mater.*, **2004**, *3*, 823.

[9] C. De Rosa, C. Park, E. L. Thomas, B. Lotz, *Nature*, **2000**, *405*, 433.

[10] J. C. Zhao, S. C. Jiang, X. L. Ji, L. J. An, B. Z. Jiang, *Polymer*, **2005**, *46*, 6513.

[11] P. Mokarian-Tabari, T. W. Collins, J. D. Holmes, M. A. Morris, *ACS Nano*, **2011**, *5*, 4617.

[12] M. J. Fasolka, A. M. Mayes, *Ann. Rev. Mater. Res.*, **2001**, *31*, 323.

[13] Q. Peng, Y. C. Tseng, S. B. Darling, J. W. Elam, *Adv. Mater.*, **2010**, *22*, 5129.

[14] B. Nandan, E. B. Gowd, N. C. Bigall, A. Eychmuller, P. Formanek, P. Simon, M. Stamm, *Adv. Funct. Mater.*, **2009**, *19*, 2805.

[15] X. D. Gu, P. Dorsey, T. P. Russell, *Adv. Mater.*, **2012**, *24*, 5505.

[16] Potemkin, II, *Macromolecules*, **2004**, *37*, 3505.

[17] R. A. Farrell, N. Petkov, M. T. Shaw, V. Djara, J. D. Holmes, M. A. Morris, *Macromolecules*, **2010**, *43*, 8651.

[18] E. Kim, H. Ahn, S. Park, H. Lee, M. Lee, S. Lee, T. Kim, E. A. Kwak, J. H. Lee, X. Lei, J. Huh, J. Bang, B. Lee, D. Y. Ryu, *ACS Nano*, **2013**, *7*, 1952.

[19] X. D. Gu, Z. W. Liu, I. Gunkel, S. T. Chourou, S. W. Hong, D. L. Olynick, T. P. Russell, *Adv. Mater.*, **2012**, *24*, 5688.

[20] R. Ruiz, R. L. Sandstrom, C. T. Black, *Adv. Mater.*, **2007**, *19*, 587.

[21] J. Xu, S. W. Hong, W. Y. Gu, K. Y. Lee, D. S. Kuo, S. G. Xiao, T. P. Russell, *Adv. Mater.*, **2011**, *23*, 5755.

[22] T. Ghoshal, T. Maity, J. F. Godsell, S. Roy, M. A. Morris, *Adv. Mater.*, **2012**, *24*, 2390.

[23] T. Ghoshal, R. Senthamaraikannan, M. T. Shaw, J. D. Holmes, M. A. Morris, *Nanoscale*, **2012**, *4*, 7743.

[24] T. Ghoshal, M. T. Shaw, C. T. Bolger, J. D. Holmes, M. A. Morris, *J. Mater. Chem.*, **2012**, *22*, 12083.

[25] V. Mishra, G. H. Fredrickson, E. J. Kramer, *ACS Nano*, **2012**, *6*, 2629.

[26] X. H. Zhang, B. C. Berry, K. G. Yager, S. Kim, R. L. Jones, S. Satija, D. L. Pickel, J. F. Douglas, A. Karim, *ACS Nano*, **2008**, *2*, 2331.

[27] J. Garcia-Turiel, B. Jerome, *Colloid Polym. Sci.*, **2007**, *285*, 1617.

[28] H. M. Mao, M. A. Hillmyer, *Macromolecules*, **2005**, *38*, 4038.

[29] Y. Y. Zhao, C. G. Bao, R. Feng, T. J. Mason, *J. Appl. Polym. Sci.*, **1998**, *68*, 1411.

[30] D. L. Ho, B. Hammouda, S. R. Kline, W. R. Chen, *J. Polym. Sci. Pt. B-Polym. Phys.*, **2006**, *44*, 557.

[31] W. Y. Chen, J. X. Zheng, S. Z. D. Cheng, C. Y. Li, P. Huang, L. Zhu, H. M. Xiong, Q. Ge, Y. Guo, R. P. Quirk, B. Lotz, L. F. Deng, C. Wu, E. L. Thomas, *Phys. Rev. Lett.*, **2004**, *93*, 028301.

[32] G. H. Michler, *Electron Microscopy of Polymers* Springer, **2008**.

[33] B. M. D. O'Driscoll, G. H. Griffiths, M. W. Matsen, I. W. Hamley, *Macromolecules*, **2011**, *44*, 8527.

[34] C. R. Martin, I. A. Aksay, *J. Electroceram.*, **2004**, *12*, 53.

[35] R. Prakash, R. J. Choudhary, L. S. S. Chandra, N. Lakshmi, D. M. Phase, *J. Phys.-Condes. Matter*, **2007**, *19*.

[36] P. Mills, J. L. Sullivan, *J. Phys. D-Appl. Phys.*, **1983**, *16*, 723.

[37] T. Fujii, F. M. F. de Groot, G. A. Sawatzky, F. C. Voogt, T. Hibma, K. Okada, *Physical Review B*, **1999**, *59*, 3195.

[38] K. Q. Peng, Y. Wu, H. Fang, X. Y. Zhong, Y. Xu, J. Zhu, *Angew. Chem.-Int. Edit.*, **2005**, *44*, 2737.
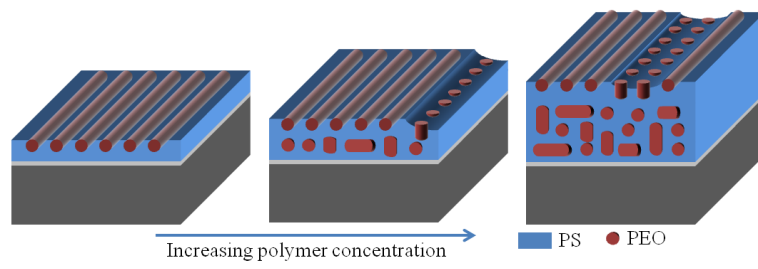
**Scheme 1.** Schematic illustration of equilibrium surface patterns, thicknesses and internal morphology for different concentrations of polymers for longer annealing time (2h).
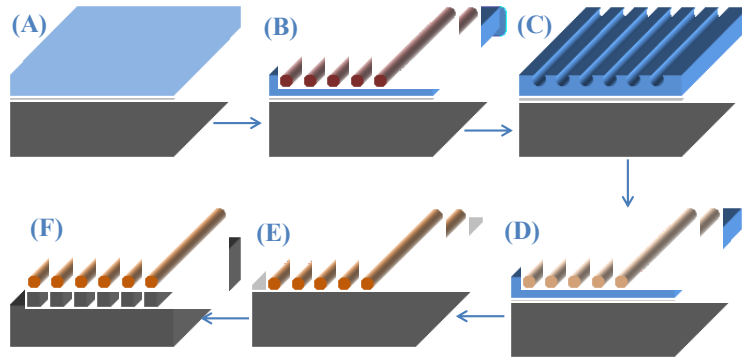
**Scheme 2**. Schematic illustration of the fabrication of horizontal ordered Si nanowires on substrate. (A) PS-PEO thin film after spin coating (B) PEO cylinders parallel to the substrate in the PS matrix after solvent annealing (C) Modification of PEO cylinders creates nanoporous template (D) Iron precursor solution spin coated on the template (E) Iron oxide nanowires formed after UV/ozone treatment (F) Si nanowires fabricated by consecutive silica and silicon ICP etch processes.
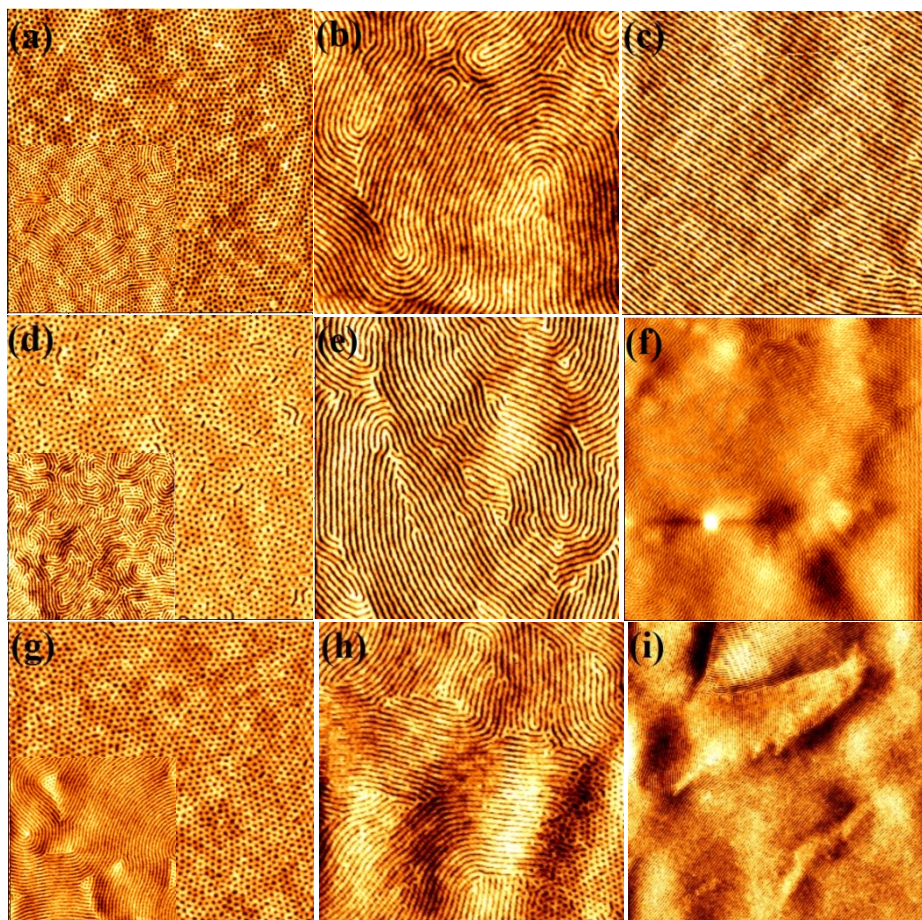
**Figure 1** Tapping mode AFM images of the solvent annealed film with (a, a-inset, b, c) 1%, (d, d-inset, e, f) 2% and (g, g-inset, h, i) 3% polymeric solution for 30m, 1h, 2h and 2h 30m respectively. All the images are 2 x 2 µm. (f) 5 x 5 µm. (i) 4 x 4 µm.
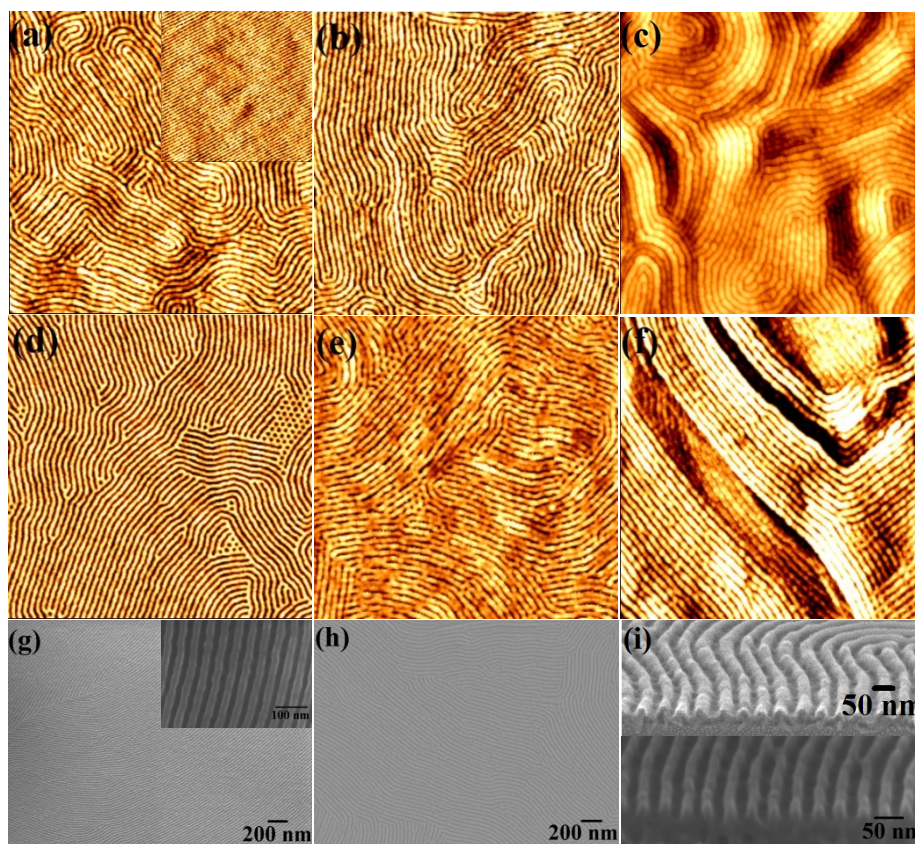
**Figure 2** AFM and SEM images of the nanoporous template after ethanol treatment for (a, a-inset, g, g-inset) 1%, (b, h) 2 % and (c) 3% polymeric solution respectively. (d) nanoporous template with mixed morphology. Ethanol treated film for (e) 1% film after 14 h and (f) 3% film after 24 h. (i) cross sectional SEM images of the template with 1% solution. All the AFM images are 2 x 2 μm.
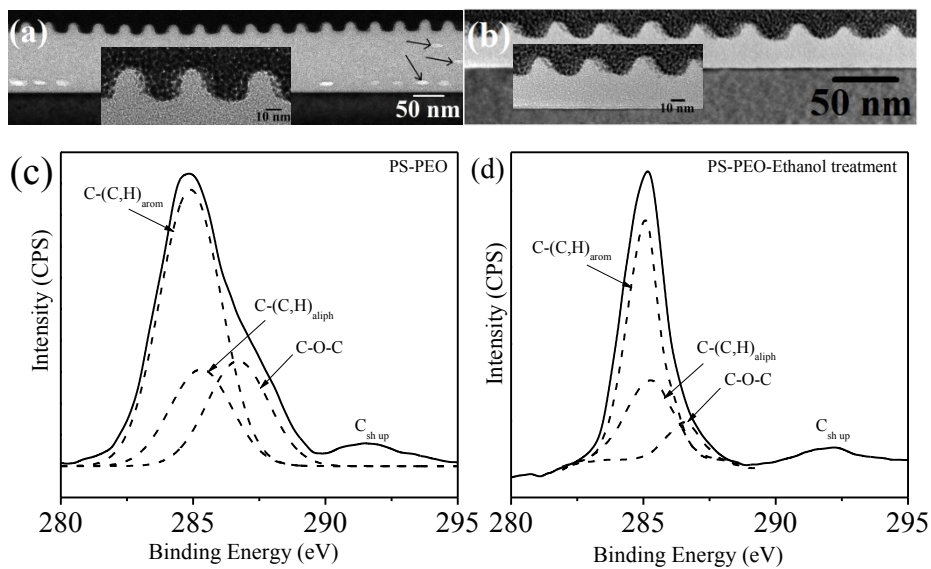
**Figure 3** FIB thinned cross sectional TEM images of the nanoporous template after ethanol treatment for (a) 3% and (b) 1% polymeric solution respectively. XPS C1s spectra for (c) PS-PEO solvent annealed and (d) ethanol treated film respectively.
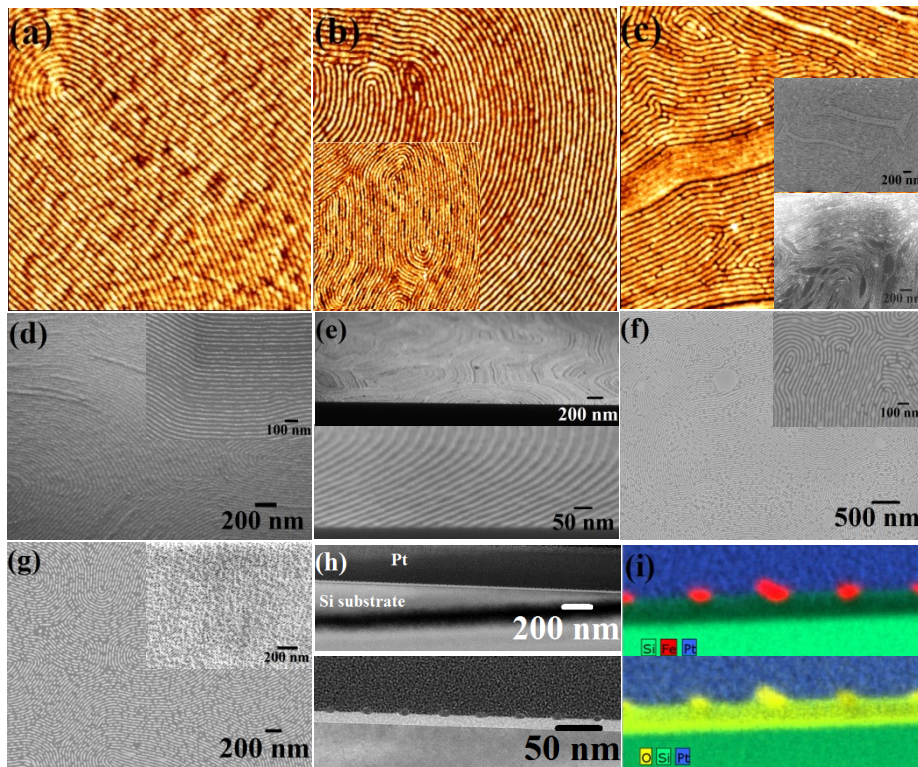
**Figure 4** Iron oxide nanowires formed after UV/Ozone treatment for different polymeric solution (a, d) 1%, (b, f) 2% and (c) 3% respecticely. Iron oxide nanowires formed annealing at 800º C for 1h for different polymeric solution (e) 1%, (f) 2% and (inset of c) 3% respecticely. Oxide nanowires prepared for different concentrations of precursor (g) 4% and (inset of g) 5% respectively. (h) Cross sectional TEM images of iron oxide nanowires. (i) elemental mapping of Fe, O and Si.
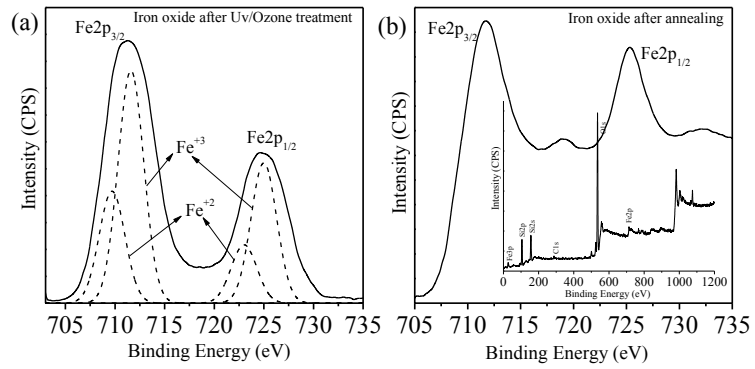
**Figure 5** Fe 2p spectra of iron oxide nanowires after (a) UV/Ozone treatment and (b) annealing at 800º C for 1h. Inset of b shows XPS Survey spectrum for the annealed sample on Si substrate.
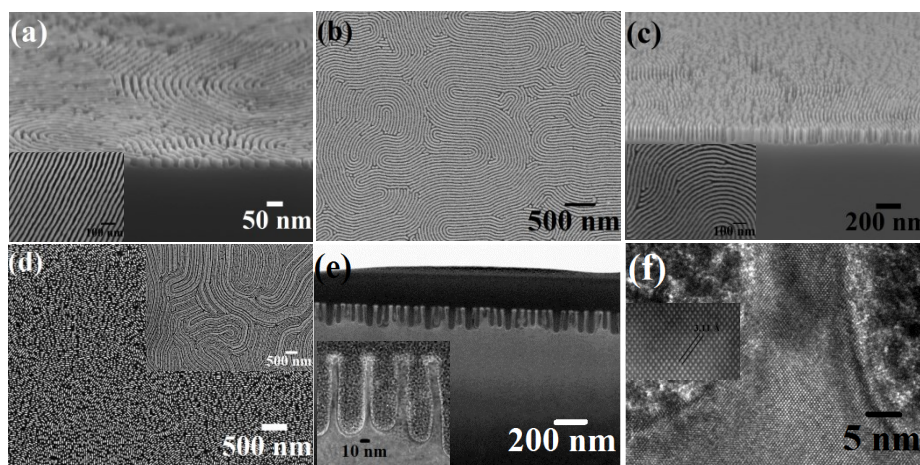
**Figure 6** SEM images of horizontal Si nanowires with iron oxide as a hard mask after (a) 1 min (b) 2 min and (c) 3 min Si etch respectively. (d) and inset shows pattern transferred nanostructures for lower and higher concentrations of precursor respectively. (e) Cross sectional TEM and (f) HRTEM images of Si nanowires after iron oxide removal.